

# The Lyman- $\alpha$ power spectrum - CMB lensing convergence cross-correlation

Chi-Ting Chiang,<sup>a</sup> and Anže Slosar<sup>b</sup>

<sup>a</sup>C.N. Yang Institute for Theoretical Physics, Stony Brook University, Stony Brook, NY 11794, U.S.A.

<sup>b</sup>Brookhaven National Laboratory, Bldg 510, Upton, NY 11375, U.S.A.

E-mail: [chi-ting.chiang@stonybrook.edu](mailto:chi-ting.chiang@stonybrook.edu), [anze@bnl.gov](mailto:anze@bnl.gov)

**Abstract.** We investigate the three-point correlation between the Lyman- $\alpha$  forest and the CMB weak lensing ( $\delta_F \delta_F \kappa$ ) expressed as the cross-correlation between the CMB weak lensing field and local variations in the forest power spectrum. In addition to the standard gravitational bispectrum term, we note the existence of a non-standard systematic term coming from mis-estimation of the mean flux over the finite length of Lyman- $\alpha$  skewers. We numerically calculate the angular cross-power spectrum and discuss its features. We integrate it into zero-lag correlation function and compare our predictions with recent results by Doux et al.. We find that our predictions are statistically consistent with the measurement, and including the systematic term improves the agreement with the measurement. We comment on the implication of the response of the Lyman- $\alpha$  forest power spectrum to the long-wavelength density perturbations.

---

## Contents

<b>1</b>	<b>Introduction</b>	<b>1</b>
<b>2</b>	<b>Underlying signal due to gravitational evolution</b>	<b>1</b>
<b>3</b>	<b>Continuum-misestimation bias due to Lyman-<math>\alpha</math> forest measurement</b>	<b>6</b>
<b>4</b>	<b>Comparison with observation</b>	<b>9</b>
4.1	Contamination from Damped Lyman- $\alpha$ systems	9
4.2	Measurement of Doux et al.	10
<b>5</b>	<b>Conclusion</b>	<b>12</b>

---

## 1 Introduction

The three-point function of the large-scale structure contains ample information that cannot be probed by the two-point function, hence it is sensitive to the nonlinear gravitational evolution [1], tracer bias [2], and even the inflationary physics [3]. Measurement of the three-point function, or its Fourier counterpart bispectrum, by auto- or cross-correlation is thus one of the biggest scientific goals for ongoing and future surveys.

In this paper, we propose a new bispectrum formed by the Lyman- $\alpha$  forest power spectrum (hereafter forest power spectrum) and the CMB lensing convergence. Since the forest power spectrum is sensitive to the small-scale matter fluctuation at  $2 \leq z \leq 4$  whereas CMB lensing convergence measures the total matter fluctuation along the line-of-sight, this combination of bispectrum allows us to probe the nonlinear structure formation that has not been explored using galaxies as tracers. Note that a similar observable has been measured in Ref. [4] by cross-correlating the one-dimensional forest power spectrum and the CMB lensing at *the same* angular position. We shall generalize the bispectrum to include the complete angular scale between the Lyman- $\alpha$  forest skewers and the CMB lensing, and demonstrate that their observable is an integral over the angular scale of the total bispectrum.

The rest of this paper is organized as follows. In Section 2, we compute the underlying signal generated by the gravitational evolution. In Section 3, we calculate the signal due to the continuum fitting when measuring the Lyman- $\alpha$  forest, which we refer to as the “continuum-misestimation bias”. In Section 4, we discuss the contamination from damped Lyman- $\alpha$  absorbers and compare our prediction with the measurement in Ref. [4]. We conclude in Section 5. Throughout the paper we adopt the Planck cosmology [5], i.e.  $h = 0.6803$ ,  $\Omega_b h^2 = 0.0226$ ,  $\Omega_c h^2 = 0.1186$ ,  $A_s = 2.137 \times 10^{-9}$ , and  $n_s = 0.9667$ .

## 2 Underlying signal due to gravitational evolution

The mean of the forest power spectrum at redshift  $z$  with width  $\Delta z$ , corresponding to the comoving distance  $r_{\parallel}$  and width  $\Delta r$ , can be written as [6]

$$P_{FF}(\mathbf{k}_s) = P_{FF}(k_s, \mu_s) = b_F^2 (1 + \beta_F \mu_s^2)^2 P_{\delta\delta}(k_s) \mathcal{D}_{\text{NL}}(k_s, \mu_s), \quad (2.1)$$

where  $\mathbf{k}_s$  is the small-scale wavevector (opposed to the large-scale mode that we introduce later),  $\mu_s$  is the cosine of  $\mathbf{k}_s$  along the line-of-sight,  $b_F$  is the flux bias,  $\beta_F$  is the redshift-space distortion parameter for the flux,  $P_{\delta\delta}$  is the linear power spectrum, and  $\mathcal{D}_{\text{NL}}$  is the fitting formula for the small-scale nonlinearity. In this paper we shall use the fitting function provided in Ref. [7] as

$$\mathcal{D}_{\text{NL}}(k_s, \mu_s) = \exp \left\{ [q_1 \Delta^2(k_s) + q_2 \Delta^4(k_s)] \left[ 1 - \left( \frac{k_s}{k_v} \right)^{a_v} \mu_s^{b_v} \right] - \left( \frac{k_s}{k_p} \right)^2 \right\}, \quad (2.2)$$

where  $\Delta^2(k) = k^3 P_{\delta\delta}(k)/(2\pi^2)$  and  $(q_1, q_2, k_v, a_v, b_v, k_p)$  are fitting parameters obtained from simulations. Note that the linear power spectrum as well as all biases and fitting parameters (provided in Table 4 and 5 of Ref. [7]) depend on redshift, but we do not write the dependence explicitly when no confusion occurs.

If there is a large-scale fluctuation on the sky, the forest power spectrum would be modulated and at the leading order the forest power spectrum at angular position  $\mathbf{r}_\perp$  becomes [8]

$$P_{FF}(\mathbf{k}_s, \mathbf{r}_\perp) = P_{FF}(\mathbf{k}_s) + \frac{dP_{FF}(\mathbf{k}_s)}{d\bar{\delta}} \bar{\delta}(\mathbf{r}_\perp), \quad (2.3)$$

where  $\bar{\delta}$  is the two-dimensional projected large-scale density fluctuation, and  $dP_{FF}(\mathbf{k}_s)/d\bar{\delta}$  is the response of the forest power spectrum with respect to  $\bar{\delta}$  due to the gravitational evolution, which can be measured from the separate universe simulations [8, 9]. In the flat-sky approximation, the three-dimensional position can be decomposed into parallel  $r_\parallel$  and transverse  $\mathbf{r}_\perp$  components, and  $\bar{\delta}$  is given by

$$\bar{\delta}(\mathbf{r}_\perp) = \frac{1}{\Delta r} \int_{r_\parallel - \Delta r/2}^{r_\parallel + \Delta r/2} dr'_\parallel \delta(r'_\parallel, \mathbf{r}_\perp) = \frac{1}{\Delta r} \int dr'_\parallel \delta(r'_\parallel, \mathbf{r}_\perp) \Theta \left( \frac{\Delta r}{2} - |r'_\parallel - r_\parallel| \right), \quad (2.4)$$

where  $\delta$  is the underlying matter density perturbation and  $\Theta$  is the heaviside step function. At the leading order, i.e in the limit where the wavevector of the large-scale mode  $\bar{\delta}$  is much smaller than  $\mathbf{k}_s$ , the response depends only on the small-scale mode  $\mathbf{k}_s$  and is independent of the wavelength of  $\bar{\delta}$ .

Consider measuring the correlation between the forest power spectrum with the two-dimensional projected CMB lensing convergence in the same redshift bin

$$\begin{aligned} \kappa(\mathbf{r}_\perp) &= \int_{r_\parallel - \Delta r/2}^{r_\parallel + \Delta r/2} dr'_\parallel \int d^2 r'_\perp \delta(\mathbf{r}') W_\kappa(r'_\parallel) \Lambda_\kappa(\mathbf{r}'_\perp - \mathbf{r}_\perp) \\ &= \int d^3 r' \delta(\mathbf{r}') W_\kappa(r'_\parallel) \Theta \left( \frac{\Delta r}{2} - |r'_\parallel - r_\parallel| \right) \Lambda_\kappa(\mathbf{r}'_\perp - \mathbf{r}_\perp), \end{aligned} \quad (2.5)$$

where  $W_\kappa$  is the lensing kernel and  $\Lambda_\kappa$  is the weighting filter in the transverse direction (which we will later set to be the Wiener filter). The lensing kernel is given by

$$W_\kappa(r_\parallel) = \frac{3H_0^2 \Omega_m}{2c^2} \frac{r_\parallel}{a(r_\parallel)} \frac{r_* - r_\parallel}{r_*}, \quad (2.6)$$

where  $H_0$  is the present-day Hubble,  $\Omega_m$  is the fractional energy density of matter,  $c$  is the speed of light,  $a$  is the scale factor, and  $r_*$  is the comoving distance to the last-scattering surface. The three-point correlation between  $P_{FF}$  and  $\kappa$  in Fourier space is thus

$$\langle P_{FF}(\mathbf{k}_s, \mathbf{k}_{l\perp}) \kappa(\mathbf{k}'_{l\perp}) \rangle' = \frac{dP_{FF}(\mathbf{k}_s)}{d\bar{\delta}} \langle \bar{\delta}(\mathbf{k}_{l\perp}) \kappa(\mathbf{k}'_{l\perp}) \rangle' = \frac{dP_{FF}(\mathbf{k}_s)}{d\bar{\delta}} P_{\bar{\delta}\kappa}^{2d}(\mathbf{k}_{l\perp}), \quad (2.7)$$

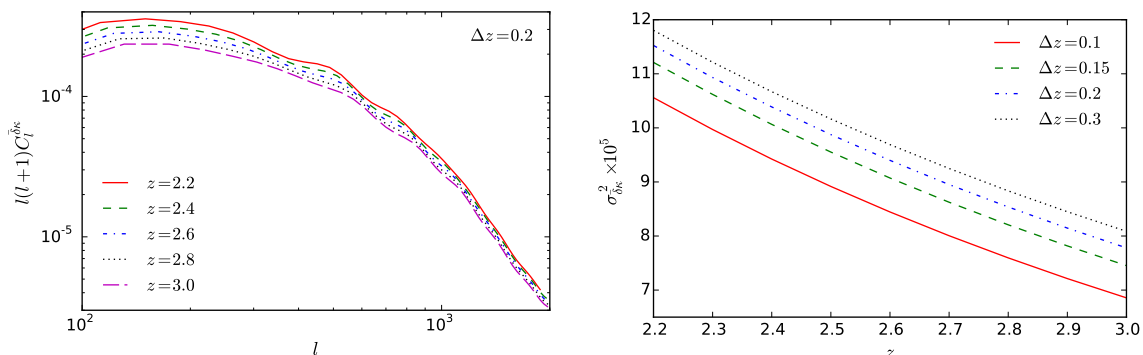


**Figure 1:** (Left) The angular power spectrum  $C_l^{\bar{\delta}\kappa}$  with  $\Delta z = 0.2$  as a function of the angular scale  $l$  at various redshifts denoted by different colors and line styles. We set  $l \geq 100$  so that the flat-sky approximation works well. (Right) The correlation of  $\bar{\delta}$  and  $\kappa$  at the same angular position,  $\sigma_{\bar{\delta}\kappa}^2$ , as a function of redshift for various  $\Delta z$  denoted by different colors and line styles.

where  $\langle \rangle'$  is the ensemble average without the Dirac delta function. Using eqs. (2.4)–(2.5), we can compute  $P_{\bar{\delta}\kappa}^{2d}$  as

$$\begin{aligned}
P_{\bar{\delta}\kappa}^{2d}(\mathbf{k}_{l\perp}) &= \int_{r_{\parallel}-\Delta r/2}^{r_{\parallel}+\Delta r/2} dr'_{1\parallel} W_{\kappa}(r'_{1\parallel}) \int dr'_{2\parallel} \frac{1}{\Delta r} \Theta\left(\frac{\Delta r}{2} - |r'_{2\parallel} - r_{\parallel}|\right) \\
&\quad \times \int \frac{dq_{\parallel}}{2\pi} P_{\delta\delta}(q_{\parallel}, \mathbf{k}_{l\perp}) \Lambda_{\kappa}(-\mathbf{k}_{l\perp}) e^{iq_{\parallel}(r'_{1\parallel} - r'_{2\parallel})} \\
&= \int_{r_{\parallel}-\Delta r/2}^{r_{\parallel}+\Delta r/2} dr'_{\parallel} W_{\kappa}(r'_{\parallel}) \int \frac{dq_{\parallel}}{2\pi} P_{\delta\delta}(q_{\parallel}, \mathbf{k}_{l\perp}) \Lambda_{\kappa}(-\mathbf{k}_{l\perp}) \text{sinc}\left(\frac{q_{\parallel}\Delta r}{2}\right) e^{iq_{\parallel}(r'_{\parallel} - r_{\parallel})}, \quad (2.8)
\end{aligned}$$

and the only assumption we make is that  $P_{\delta\delta}$  is independent of  $z$  within  $\Delta z$ . Because of the sinc function, the contribution to  $P_{\bar{\delta}\kappa}^{2d}$  from the parallel mode is mainly from  $q_{\parallel} \lesssim \Delta r^{-1}$ . Physically, this means that  $P_{\bar{\delta}\kappa}^{2d}$  is sensitive to the largest parallel mode, which is set by the redshift bin size. Following Ref. [10], in the flat-sky approximation we can convert the two-dimensional power spectrum to the angular power spectrum as

$$l(l+1)C_l^{\bar{\delta}\kappa} \approx k_{l\perp}^2 P_{\bar{\delta}\kappa}^{2d}(\mathbf{k}_{l\perp}), \quad (2.9)$$

where  $l + 1/2 \approx r_{\parallel} k_{l\perp}$ . Combining eqs. (2.7)–(2.9), we have the most general correlation between forest power spectrum and CMB lensing convergence, which includes both the dependence on the small-scale mode  $\mathbf{k}_s$  and the large-scale mode  $\mathbf{k}_{l\perp}$ , or equivalently the angular scale  $l$ . This calculation is general and can be used for other fields in place of Lyman- $\alpha$ , most notably 21-cm emission from intensity mapping.

The left panel of figure 1 shows  $C_l^{\bar{\delta}\kappa}$  with  $\Delta z = 0.2$  as a function of the angular scale  $l$  at various redshifts. We set  $l \geq 100$  so that the flat-sky approximation works well. To numerically evaluate  $C_l^{\bar{\delta}\kappa}$ , we set  $q_{\parallel, \text{max}} = 1000 h \text{ Mpc}^{-1}$  and confirm that the result is insensitive to the choice of  $q_{\parallel, \text{max}}$ . We also take  $W_{\kappa}$  to be the Wiener filter from Ref. [11] with  $l = r'_{\parallel} k_{l\perp}$ . The power spectrum is larger at lower redshift, and this is the result of the gravitational evolution. To check the approximation that the linear power spectrum does not

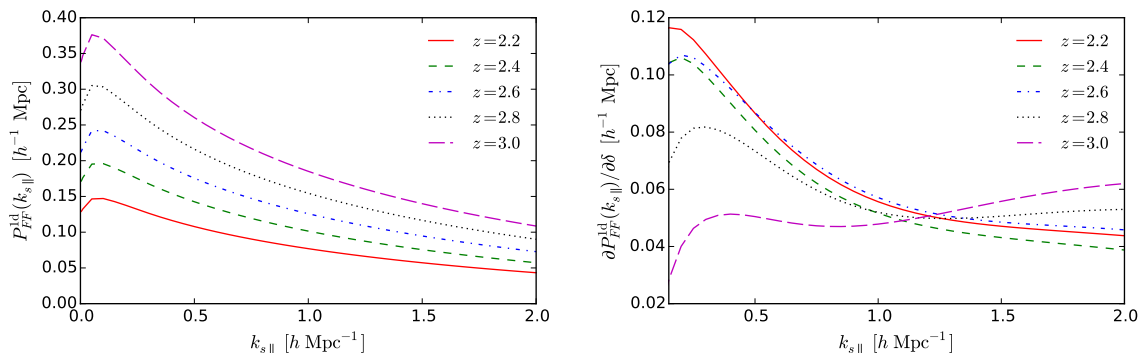


**Figure 2:** (Left) One-dimensional Lyman- $\alpha$  forest power spectrum at different redshifts. (Right) Response of the one-dimensional Lyman- $\alpha$  forest power spectrum to long-wavelength overdensity evaluated with the separate universe simulations and eq. (2.11).

vary within the redshift bin  $\Delta z$ , we include the redshift evolution and find that the fractional difference is less than 1%. The agreement is slightly better at higher redshift since  $\Delta r$  is smaller at larger  $z$  when  $\Delta z$  is fixed.

Since the forest power spectrum is frequently measured as the one-dimensional power spectrum, we can Fourier transform in the small-scale transverse direction:

$$P_{FF}^X(k_{s\parallel}, \mathbf{r}_{s\perp}) = \int \frac{d^2 k_{s\perp}}{(2\pi)^2} P_{FF}(k_{s\parallel}, \mathbf{k}_{s\perp}) e^{i\mathbf{k}_{s\perp} \cdot \mathbf{r}_{s\perp}}, \quad (2.10)$$

with the one-dimensional power spectrum given by  $P_{FF}^{1d}(k_{s\parallel}) = P_{FF}^X(k_{s\parallel}, \mathbf{r}_{s\perp} = 0)$ . Similarly one can Fourier transform the cross-correlation of eq. (2.7) in the small-scale transverse wavevector  $\mathbf{k}_{s\perp}$  to get a cross-correlation as a function of  $(k_{s\parallel}, \mathbf{r}_{s\perp}, k_{l\perp})$ . This tells us how a cross-power spectrum between two close skewers as a function of the small-scale parallel wavevector  $k_{s\parallel}$  and small-scale perpendicular separation  $\mathbf{r}_{s\perp}$  responds to a large-scale mode in  $\kappa$  field fluctuation. For this we need

$$\begin{aligned} \frac{dP_{FF}^X(k_{s\parallel}, \mathbf{r}_{s\perp})}{d\bar{\delta}} &= \int \frac{d^2 k_{s\perp}}{(2\pi)^2} \frac{dP_{FF}(k_{s\parallel}, \mathbf{k}_{s\perp})}{d\bar{\delta}} e^{i\mathbf{k}_{s\perp} \cdot \mathbf{r}_{s\perp}} \\ &= \int \frac{d^2 k_{s\perp}}{(2\pi)^2} P_{FF}(k_{s\parallel}, \mathbf{k}_{s\perp}) \frac{d \ln P_{FF}(k_{s\parallel}, \mathbf{k}_{s\perp})}{d\bar{\delta}} e^{i\mathbf{k}_{s\perp} \cdot \mathbf{r}_{s\perp}}. \end{aligned} \quad (2.11)$$

As before, the one-dimensional specialization is just the case when we set  $\mathbf{r}_{s\perp} = 0$ , i.e.  $dP_{FF}^{1d}(k_{s\parallel})/d\bar{\delta} = dP_{FF}^X(k_{s\parallel}, \mathbf{r}_{s\perp} = 0)/d\bar{\delta}$ .

To numerically evaluate the one-dimensional forest power spectrum, we use eqs. (2.1)–(2.2) and set  $k_{s\perp, \text{max}} = 1000 h \text{Mpc}^{-1}$ . To compute the response of the one-dimensional forest power spectrum, we first measure and smooth  $d \ln P_{FF}(k_{s\parallel}, \mathbf{k}_{s\perp})/d\bar{\delta}$  from the separate universe simulations as described in Refs. [8, 9] and then use the analytic form of  $P_{FF}(k_{s\parallel}, \mathbf{k}_{s\perp})$ , i.e. eqs. (2.1)–(2.2). To minimize the possible bias on the integration from the smoothing and interpolation, we set  $k_{s\perp, \text{max}} = 10 h \text{Mpc}^{-1}$ . Figure 2 shows the one-dimensional forest power spectrum (left) and its response to  $\bar{\delta}$  (right). The one-dimensional forest power spectrum is larger at higher redshift due to the increase of  $|b_F|$ . Conversely, the response of the one-dimensional forest power spectrum, which contains the responses from

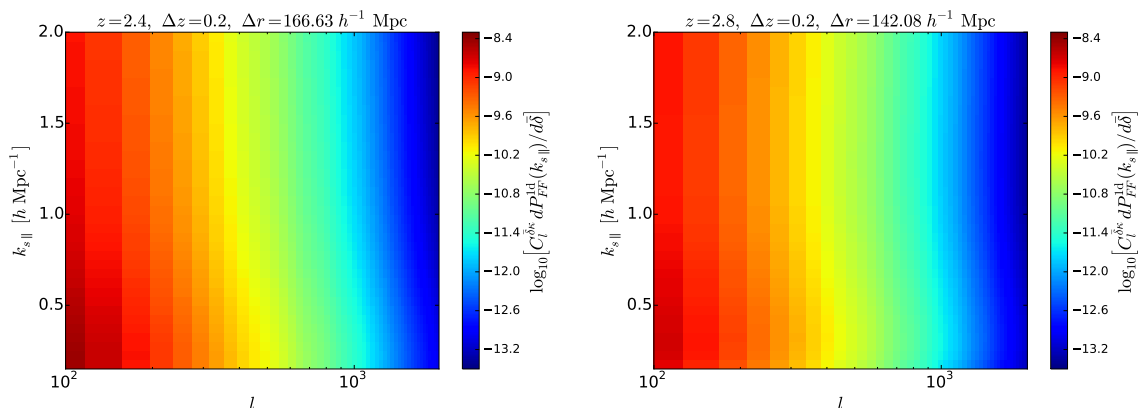


**Figure 3:** Correlation of the one-dimensional Lyman- $\alpha$  forest power spectrum and the CMB lensing convergence at  $z = 2.4$  (left) and  $2.8$  (right) assuming  $\Delta z = 0.2$ , which corresponds respectively to  $\Delta r = 166.63$  and  $142.08 h \text{ Mpc}^{-1}$ .  $l$  is the angular scale between the skewer and the lensing convergence, and  $k_{s\parallel}$  is the scale of the one-dimensional Lyman- $\alpha$  forest power spectrum.

linear power spectrum, flux bias, and the nonlinear fitting function, is larger at lower redshift for  $k \lesssim 1 h \text{ Mpc}^{-1}$ .

To evaluate the correlation between the one-dimensional forest power spectrum and the CMB lensing convergence, we take the product of  $C_l^{\delta\kappa}$  from the left panel of figure 1 and  $dP_{FF}^{1d}(k_{s\parallel})/d\bar{\delta}$  from the right panel of figure 2. Figure 3 shows the result at  $z = 2.4$  (left) and  $2.8$  (right) as a function of  $l$  (the angular scale between the skewer and the lensing convergence) and  $k_{s\parallel}$  (the scale of the one-dimensional forest power spectrum), assuming  $\Delta z = 0.2$ , which corresponds respectively to  $\Delta r = 166.63$  and  $142.08 h \text{ Mpc}^{-1}$ . We find that at both redshifts the scale dependence on  $l$  and  $k_{s\parallel}$  is similar, and the more apparent difference is the amplitude of the signal. Specifically, at lower redshift the signal is larger, which is likely due to the stronger gravitational evolution.

Lastly, if the correlation between the one-dimensional forest power spectrum ( $\mathbf{r}_{s\perp} = 0$ ) and the lensing convergence is measured in configuration space, then we can also Fourier transform the *large-scale*  $\mathbf{k}_{l\perp}$ :

$$\begin{aligned} \langle P_{FF}^{1d}(k_{s\parallel}, \mathbf{r}_{\perp}) \kappa(\mathbf{r}'_{\perp}) \rangle &= \int \frac{d^2 \mathbf{k}_{l\perp}}{(2\pi)^2} \langle P_{FF}^{1d}(k_{s\parallel}, \mathbf{k}_{l\perp}) \kappa(\mathbf{k}_{l\perp}) \rangle e^{i\mathbf{k}_{l\perp} \cdot (\mathbf{r}_{\perp} - \mathbf{r}'_{\perp})} \\ &= \frac{dP_{FF}^{1d}(k_{s\parallel})}{d\bar{\delta}} \int \frac{d^2 \mathbf{k}_{l\perp}}{(2\pi)^2} P_{\delta\kappa}^{2d}(\mathbf{k}_{l\perp}) e^{i\mathbf{k}_{l\perp} \cdot (\mathbf{r}_{\perp} - \mathbf{r}'_{\perp})}. \end{aligned} \quad (2.12)$$

Furthermore, if the correlations are only measured at the same angular position ( $\mathbf{r}_{\perp} = \mathbf{r}'_{\perp}$ ), as done in Ref. [4], then the relevant quantity in this case is the Fourier transform of  $\bar{P}_{\delta\kappa}^{2d}$  evaluated at zero lag, i.e.

$$\sigma_{\delta\kappa}^2 = \int \frac{d^2 \mathbf{k}_{l\perp}}{(2\pi)^2} P_{\delta\kappa}^{2d}(\mathbf{k}_{l\perp}), \quad (2.13)$$

which the variance of the  $\bar{\delta\kappa}$  field. Note that while this is the region where majority of signal to noise is concentrated, there is in principle more information available in the data.

We show the correlation at the same angular position in the right panel of figure 1 as a function of redshift for various  $\Delta z$ . We confirm that the results are insensitive to the choice of  $k_{\max}$  for the integration and the redshift evolution of  $P_{\delta\delta}$ . As for  $C_l^{\delta\kappa}$ ,  $\sigma_{\delta\kappa}^2$  is larger at lower redshift due to the gravitational evolution. Interestingly, while the comoving distances between  $\Delta z = 0.1$  and  $0.3$  differ by a factor of three, the change in  $\sigma_{\delta\kappa}^2$  is only from 12 to 18%. Should we compute

$$\sigma_{\delta\delta}^2 = \int \frac{d^3 k_l}{(2\pi)^3} P_{\delta\delta}(k_l) \text{sinc}^2\left(\frac{k_{l\parallel} \Delta r}{2}\right), \quad (2.14)$$

we have  $\sigma_{\delta\delta}^2(\Delta z = 0.1)/\sigma_{\delta\delta}^2(\Delta z = 0.3) \approx 2.9$  between  $2.2 \leq z \leq 3.0$ . This is because  $\sigma_{\delta\delta}^2$  is the variance of  $\delta$  for a parallel scale  $\Delta r$ , and the larger the  $\Delta r$  the smaller the variance. On the other hand,  $\sigma_{\delta\kappa}^2$  includes the integral of lensing kernel along the line-of-sight, and the larger the  $\Delta r$  the larger the lensing contribution. These two effects roughly cancel each other, as a result  $\sigma_{\delta\kappa}^2$  is much less affected by the width in the line-of-sight direction.

### 3 Continuum-misestimation bias due to Lyman- $\alpha$ forest measurement

In the previous section we compute the gravitational bispectrum of flux-flux-lensing. In this section we shall discuss a non-standard systematic term coming from the mis-estimation of the mean flux over the finite length of Lyman- $\alpha$  forest skewers, which we shall refer to as the ‘‘continuum-misestimation bias’’.

Intuitively, this effect comes from the fact that over the length of the forest, one cannot distinguish between a large-scale absorption that would lower the measured flux in all pixels and the change in the brightness of the quasars that would do exactly the same. Of course, using information outside the quasar allows one to, in principle, recover some of this information, but in practice this introduces large amounts of noise in the continuum calibration. Therefore, most analysis just *fit* for the quasar brightness within the forest, in effect nulling large-scale flux fluctuations modes, which leads to two effects: i) distortion of measured large-scale power spectra or correlation functions (see e.g. [12, 13]) and ii) modulation of the local small scale power spectrum normalization by the large scale mode [14]. The second effect is the one that affects the calculation in this paper as we discuss next.

The observed Lyman- $\alpha$  flux can be modeled as

$$F(r_{\parallel}, \mathbf{r}_{\perp}) = A(\mathbf{r}_{\perp}) \bar{C} \bar{F}(r_{\parallel}) [1 + \delta_F(r_{\parallel}, \mathbf{r}_{\perp})] + \epsilon, \quad (3.1)$$

where  $A$  describes the brightness of the quasar so depends on the angular position,  $\bar{C}$  is the mean continuum shape obtained from stacking all skewers in the survey,  $\bar{F}$  is the true mean flux which is independent of the angular position on the sky,  $\delta_F$  is the true flux fluctuation around  $\bar{F}$ , and  $\epsilon$  is the noise. To measure  $\delta_F$ , one performs the continuum fitting on a skewer by adjusting  $A$  until the integral of  $\delta_F$  becomes zero across this skewer. In other words, for a skewer at  $\mathbf{r}_{\perp}$  we estimate the quasar brightness as

$$\begin{aligned} \hat{A}(\mathbf{r}_{\perp}) &= \frac{1}{\Delta\tilde{r}} \int_{r_{\parallel}-\Delta\tilde{r}/2}^{r_{\parallel}+\Delta\tilde{r}/2} dr'_{\parallel} \frac{F(r'_{\parallel}, \mathbf{r}_{\perp})}{\bar{C}(r'_{\parallel}) \bar{F}(r'_{\parallel})} = A(\mathbf{r}_{\perp}) \left[ 1 + \frac{1}{\Delta\tilde{r}} \int_{r_{\parallel}-\Delta\tilde{r}/2}^{r_{\parallel}+\Delta\tilde{r}/2} dr'_{\parallel} \delta_F(r'_{\parallel}, \mathbf{r}_{\perp}) \right] \\ &= A(\mathbf{r}_{\perp}) [1 + \Delta_F(r_{\parallel}, \mathbf{r}_{\perp}, \Delta\tilde{r})], \end{aligned} \quad (3.2)$$

where  $r_{\parallel}$  and  $\Delta\tilde{r}$  are the center and the width of the skewer. Note that the typical size of  $\Delta\tilde{r}$  is 280 to 420  $h^{-1}$  Mpc [4], so  $\Delta\tilde{r}$  is generally larger than the size of the redshift bin

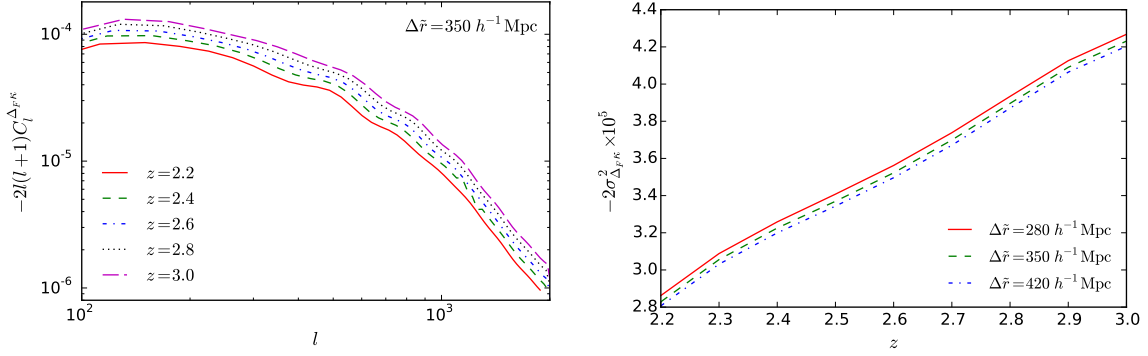


**Figure 4:** (Left) The angular power spectrum of the continuum-misestimation bias  $C_l^{\Delta_F \kappa}$  with the length of the forest  $\Delta\tilde{r} = 350 h^{-1} \text{ Mpc}$  as a function of the angular scale  $l$  at various redshifts denoted by different colors and line styles. (Right) The correlation between  $\Delta_F$  and  $\kappa$  at the same angular position,  $\sigma_{\Delta_F \kappa}^2$ , as a function of redshift for various lengths of the forest  $\Delta\tilde{r}$  denoted by different colors and line styles.

$\Delta r$ . Plugging the estimated quasar luminosity  $\hat{A}$  into the flux, we find the estimated flux perturbation at  $\mathbf{r}_\perp$  to be (ignoring the  $r_\parallel$  dependence in  $\Delta_F$  as it only describes the center of the forest)

$$\begin{aligned} \hat{\delta}_F(r'_\parallel, \mathbf{r}_\perp) &= \frac{F(r'_\parallel, \mathbf{r}_\perp)}{\hat{A}(\mathbf{r}_\perp) \bar{C}(r'_\parallel) \bar{F}(r'_\parallel)} - 1 = \frac{1 + \delta_F(r'_\parallel, \mathbf{r}_\perp)}{1 + \Delta_F(\mathbf{r}_\perp, \Delta\tilde{r})} - 1 \\ &\approx \delta_F(r'_\parallel, \mathbf{r}_\perp) [1 - \Delta_F(\mathbf{r}_\perp, \Delta\tilde{r})] - \Delta_F(\mathbf{r}_\perp, \Delta\tilde{r}). \end{aligned} \quad (3.3)$$

Note that the last term in eq. (3.3) is a constant at this angular position of  $\mathbf{r}_\perp$ , hence it contributes only to  $\mathbf{k}_s = 0$  mode of  $\hat{\delta}_F$  in Fourier space. We shall ignore it as we are interested in the forest power spectrum with  $k_s > 0$ , and to the leading order the estimated forest power spectrum of this skewer becomes

$$\hat{P}_{FF}(\mathbf{k}_s, \mathbf{r}_\perp) = \langle \hat{\delta}_F(\mathbf{k}_s, \mathbf{r}_\perp) \hat{\delta}_F(\mathbf{k}'_s, \mathbf{r}_\perp) \rangle' = P_{FF}(\mathbf{k}_s) [1 - 2\Delta_F(\mathbf{r}_\perp, \Delta\tilde{r})], \quad (3.4)$$

where the ensemble average is taken for the small-scale mode  $\mathbf{k}_s$  while keeping the large-scale  $\Delta_F$  fixed. Physically, the correction term appears because we use the *local* instead of the *global* mean flux (which is independent of  $\mathbf{r}_\perp$ ) to compute the fluctuation. The same effect is also discussed in Ref. [15] for the measurement of the position-dependent correlation function. Moreover, the larger the  $\Delta\tilde{r}$  the smaller the correction.

Though for each skewer the estimated forest power spectrum is biased, the total estimated forest power spectrum is still unbiased at the first order since  $\langle \Delta_F \rangle = 0$ . It is well known that there are corrections at the second order [14]. However, if we measure the correlation between the forest power spectrum of each skewer and the CMB lensing convergence, the signal would be biased due to the correlation between  $\Delta_F$  and  $\kappa$  at the first order. Specifically, if we consider the angular power spectrum between the forest power spectrum and the lensing convergence, then the continuum-misestimation bias is

$$\langle \hat{P}_{FF}(\mathbf{k}_s, \mathbf{k}_{l\perp}) \kappa(\mathbf{k}'_{l\perp}) \rangle' = -2P_{FF}(\mathbf{k}_s) \langle \Delta_F(\mathbf{k}_{l\perp}, \Delta\tilde{r}) \kappa(\mathbf{k}'_{l\perp}) \rangle' = -2P_{FF}(\mathbf{k}_s) P_{\Delta_F \kappa}^{2d}(\mathbf{k}_{l\perp}), \quad (3.5)$$

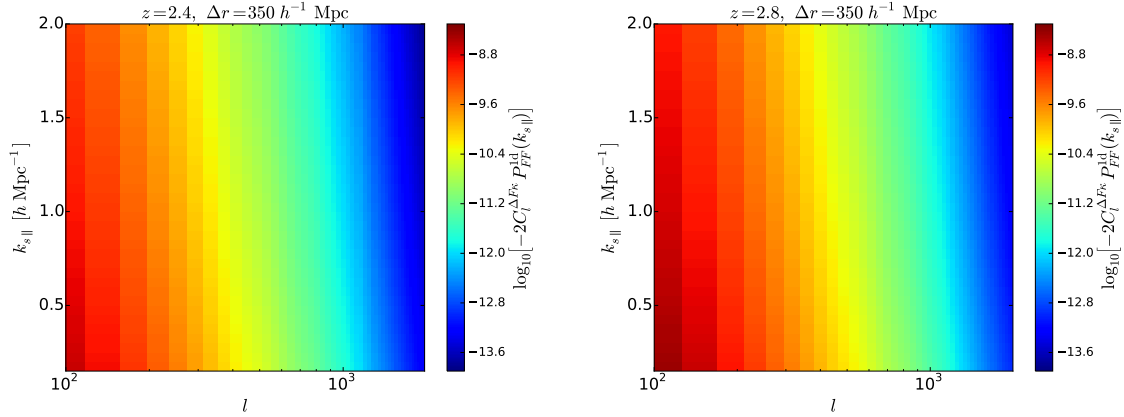


**Figure 5:** Continuum-misestimation bias of the correlation between the one-dimensional Lyman- $\alpha$  forest power spectrum and the lensing convergence due to the continuum fitting at  $z = 2.4$  (left) and  $2.8$  (right), assuming the length of the forest to be  $350 h^{-1}$  Mpc. The bias signal is plotted as a function of  $l$ , which is the angular scale between the skewer and the lensing convergence, and  $k_{s\parallel}$ , which is the scale of the one-dimensional Lyman- $\alpha$  forest power spectrum.

where

$$P_{\Delta F\kappa}^{2d}(\mathbf{k}_{l\perp}) = \int_{r_{\parallel}-\Delta\tilde{r}/2}^{r_{\parallel}+\Delta\tilde{r}/2} dr'_{\parallel} W_{\kappa}(r'_{\parallel}) \int \frac{dq_{\parallel}}{2\pi} P_{\delta F}(q_{\parallel}, \mathbf{k}_{l\perp}) \Lambda_{\kappa}(-\mathbf{k}_{l\perp}) \text{sinc}\left(\frac{q_{\parallel}\Delta\tilde{r}}{2}\right) e^{iq_{\parallel}(r'_{\parallel}-r_{\parallel})}, \quad (3.6)$$

with  $P_{\delta F}(\mathbf{k}) = [P_{\delta\delta}(\mathbf{k})P_{FF}(\mathbf{k})]^{1/2}$  in linear theory. Note that eq. (3.6) is basically the same as eq. (2.8), except for different power spectra as well as the lengths appearing in the integration boundary and the sinc function. The left panel of figure 4 shows the angular power spectrum of the continuum-misestimation bias  $C_l^{\Delta F\kappa}$  under the flat-sky approximation with  $\Delta\tilde{r} = 350 h^{-1}$  Mpc as a function of the angular scale  $l$  at various redshifts. Unlike  $C_l^{\delta\kappa}$  shown in figure 1, we find that the continuum-misestimation bias is larger at higher redshift, which is due to the fact that  $C_l^{\Delta F\kappa}$  is proportional to  $b_F$  and  $|b_F|$  is larger at higher redshift.

For the correlation between the one-dimensional forest power spectrum and the lensing convergence, the continuum-misestimation bias becomes  $-2P_{FF}^{1d}(\mathbf{k}_s)P_{\Delta F\kappa}^{2d}(\mathbf{k}_{l\perp})$ . To evaluate the signal, we take the one-dimensional forest power spectrum from the left panel of figure 2 and  $C_l^{\Delta F\kappa}$  from the right panel of figure 4, and the result is shown in figure 5 at  $z = 2.4$  (left) and  $2.8$  (right), assuming the length of the forest to be  $350 h^{-1}$  Mpc. We find that the scale dependences of the true signal and the continuum-misestimation bias are similar. This is because the scale dependences are predominantly determined by  $C_l^{\delta\kappa}$  and  $C_l^{\Delta F\kappa}$ , and the primary difference between the two angular power spectra is the flux bias as on large scale  $\mathcal{D}_{NL} \rightarrow 1$ . More interestingly, the relative contribution of the continuum-misestimation bias becomes larger at higher redshift, which is the result of increasing  $|b_F|$  at higher redshift.

Finally, for the correlation measured in configuration space at the same angular position, the continuum-misestimation bias is  $-2P_{FF}^{1d}(k_{s\parallel})\sigma_{\Delta F\kappa}^2$ , where  $\sigma_{\Delta F\kappa}^2$  is the Fourier transform of  $P_{\Delta F\kappa}^{2d}(\mathbf{k}_{l\perp})$  at zero lag, i.e.

$$\sigma_{\Delta F\kappa}^2 = \int \frac{d^2k_{l\perp}}{(2\pi)^2} P_{\Delta F\kappa}^{2d}(\mathbf{k}_{l\perp}). \quad (3.7)$$

The right panel of figure 4 shows  $\sigma_{\Delta_F \kappa}^2$  as a function of redshift for various  $\Delta \tilde{r}$ . We find that as the left panel the continuum-misestimation bias is larger at high redshift due to the larger bias. Also,  $\sigma_{\Delta_F \kappa}^2$  is almost unchanged between  $\Delta \tilde{r} = 280$  to  $420 h^{-1}$  Mpc. This is not surprising because the integration over the lensing kernel cancels the effect from the variance of the density perturbation  $\sigma_{\delta \bar{\delta}}^2$ , as we have discussed in Section 2. It is, however, interesting in the sense that in a Lyman- $\alpha$  survey the lengths of the forest may vary a lot, but to model the continuum-misestimation bias of the lensing-flux-flux bispectrum we only need one typical length for the forest, hence the modeling is simpler.

## 4 Comparison with observation

How does our prediction compare to the measurement? In this section we shall first discuss the contamination from damped Lyman- $\alpha$  systems that cannot be removed perfectly in observation, and then compare our prediction to the measured correlation between the one-dimensional forest power spectrum and CMB lensing convergence done in Ref. [4].

### 4.1 Contamination from Damped Lyman- $\alpha$ systems

In the Lyman- $\alpha$  forest measurement, the largely broadened damping wings produced by high neutral hydrogen column density systems with  $N_{HI} > 2 \times 10^{20} \text{ cm}^{-2}$ , which is known as the damped Lyman- $\alpha$  absorbers (DLAs), are discarded to avoid contamination on the forest power spectrum. However, systems such as Lyman-limit systems and sub-DLAs with less column density than DLAs but still higher than that of the Lyman- $\alpha$  forest have less prominent features hence are difficult to remove. The presence of these systems may affect the forest power spectrum and so its correlation with the lensing convergence, and we shall quantify the effect.

As pointed out in Ref. [16], the dominant effect of the high column density systems is to add power to the forest power spectrum due to their random distribution. In the limit that the number of the systems are small (typically in one skewer one in 100-1000 pixels is in the high column density system), the power is proportional to the number density of such systems. As a result, in the presence of a large-scale fluctuation  $\bar{\delta}$ , the leading order correction to the one-dimensional forest power spectrum due to the high column density systems is given by

$$P_{\text{DLA}}^{\text{1d}}(k_{s\parallel}, \mathbf{r}_{\perp}) = [1 + b_{\text{DLA}} \bar{\delta}(\mathbf{r}_{\perp})] P_{\text{DLA}}^{\text{1d}}(k_{s\parallel}), \quad (4.1)$$

where  $P_{\text{DLA}}^{\text{1d}}$  and  $b_{\text{DLA}}$  are the one-dimensional power spectrum and the bias of the high column density systems. Correlating this with the lensing convergence, the general three-point function containing the angular scale between the small-scale one-dimensional DLA power spectrum and the lensing convergence is

$$\langle P_{\text{DLA}}^{\text{1d}}(k_{s\parallel}, \mathbf{k}_{l\perp}) \kappa(\mathbf{k}'_{l\perp}) \rangle' = b_{\text{DLA}} P_{\text{DLA}}^{\text{1d}}(k_{s\parallel}) P_{\delta\kappa}^{\text{2d}}(\mathbf{k}_{l\perp}). \quad (4.2)$$

If the correlation is computed as the same angular position, then the signal becomes

$$\langle P_{\text{DLA}}^{\text{1d}}(k_{s\parallel}, \mathbf{r}_{\perp}) \kappa(\mathbf{r}_{\perp}) \rangle = b_{\text{DLA}} P_{\text{DLA}}^{\text{1d}}(k_{s\parallel}) \sigma_{\delta\kappa}^2. \quad (4.3)$$

To evaluate this signal, we need both the bias and the one-dimensional power spectrum of DLAs. Ref. [17] has measured  $b_{\text{DLA}}$  by cross-correlating DLAs with Lyman- $\alpha$  forest, and

we should take their central value  $b_{\text{DLA}} = 2.17$ , assuming that the redshift-space distortion parameter of DLAs is subdominant. For the DLA power spectrum, we use the fitting function provided in Ref. [18] describing the ratio between  $P_{\text{DLA}}^{\text{1d}}$  and  $P_{FF}^{\text{1d}}$ , and we utilize our fiducial forest power spectrum. Note that we only consider the contributions from Lyman-limit systems and sub-DLAs (i.e. the red line in figure 5 of Ref. [18]), as the prominent DLAs are discarded in Ref. [4].

## 4.2 Measurement of Doux et al.

In Ref. [4], the first detection of the correlation between the one-dimensional forest power spectrum from SDSS-III Baryon Oscillation Spectroscopic Survey Data Release 12 [19, 20] and the CMB lensing convergence from Planck [11] at the same line-of-sight is reported with a significance of  $5 \sigma$ . The authors interpreted this signal to be the response of the forest power spectrum to a large-scale overdensity, and subtracting the contribution from the leading-order squeezed-limit matter bispectrum they measured the “effective nonlinear bias”, which contains the nonlinearity such as redshift-space distortion and nonlinear clustering of gas. We shall compare the measurement of  $\langle P_{FF}^{\text{1d}}(k_{s\parallel}, \mathbf{r}_{\perp}) \kappa(\mathbf{r}_{\perp}) \rangle$  with our prediction.

Let us first compute all components of the signal. The true signal is produced by the nonlinear gravitational evolution and given by  $[dP_{FF}^{\text{1d}}(k_{s\parallel})/d\bar{\delta}] \sigma_{\bar{\delta}\kappa}^2$ , where the  $dP_{FF}^{\text{1d}}(k_{s\parallel})/d\bar{\delta}$  and  $\sigma_{\bar{\delta}\kappa}^2$  are taken from the right panel of figure 2 and the right panel of figure 1, respectively. The continuum-misestimation bias is due to the Lyman- $\alpha$  forest continuum fitting and given by  $-2P_{FF}^{\text{1d}}(k_{s\parallel})\sigma_{\Delta_{F\kappa}}^2$ , where  $P_{FF}^{\text{1d}}(k_{s\parallel})$  and  $\sigma_{\Delta_{F\kappa}}^2$  are taken from the left panel of figure 2 and the right panel of figure 4. Finally, the DLA contamination is given by  $b_{\text{DLA}}P_{\text{DLA}}^{\text{1d}}(k_{s\parallel})\sigma_{\bar{\delta}\kappa}^2$ , where  $b_{\text{DLA}} = 2.17$  and  $P_{\text{DLA}}^{\text{1d}}(k_{s\parallel})$  is taken from the fitting function in Ref. [18]. Thus, we predict the total signal of the correlation between the one-dimensional forest power spectrum and the lensing convergence from the same line-of-sight to be

$$\frac{dP_{FF}^{\text{1d}}(k_{s\parallel})}{d\bar{\delta}} \sigma_{\bar{\delta}\kappa}^2 - 2P_{FF}^{\text{1d}}(k_{s\parallel})\sigma_{\Delta_{F\kappa}}^2 + b_{\text{DLA}}P_{\text{DLA}}^{\text{1d}}(k_{s\parallel})\sigma_{\bar{\delta}\kappa}^2. \quad (4.4)$$

Figure 6 shows the different components of the cross-correlation between lensing convergence and the forest power spectrum at the same angular position for various redshifts. We first find that the DLA contamination is only important on large scales, and for  $k_{s\parallel} \gtrsim 0.6 h \text{ Mpc}^{-1}$  the contribution becomes negligible. This is due to the shape of the DLA power spectrum, which can be seen in figure 5 of Ref. [18]. Next, we find that true signal dominates over the continuum-misestimation bias at lower redshift, but the trend reverses at high redshift. This is due to the increase of the Lyman- $\alpha$  flux bias, which enhances both  $P_{FF}^{\text{1d}}(k_{s\parallel})$  and  $\sigma_{\Delta_{F\kappa}}^2$ , as well as the decrease of the forest power spectrum response. The fact that the continuum-misestimation bias is larger than the true signal at  $z \geq 2.8$  means that a large portion of the measured signal is coming from the mis-estimation of mean flux over the finite length of Lyman- $\alpha$  forest skewers, which needs to be removed for unbiasedly extracting the three-point function due to the gravitational evolution. Interestingly, the total signal shows a mild redshift evolution between  $z = 2.2$  and  $3.0$ . However, due to the lack of snapshots of separate universe simulations at  $z \geq 3$  we cannot examine this correlation at higher redshift where some of the forests are observed.

Since Ref. [4] measures the correlation from all redshifts between  $2.1 \leq z \leq 3.6$ , we shall combine the total signals at different redshifts in figure 6 into one line in order to compare with the measurement. We use the weight given in eq. (18) of Ref. [4], assuming that the

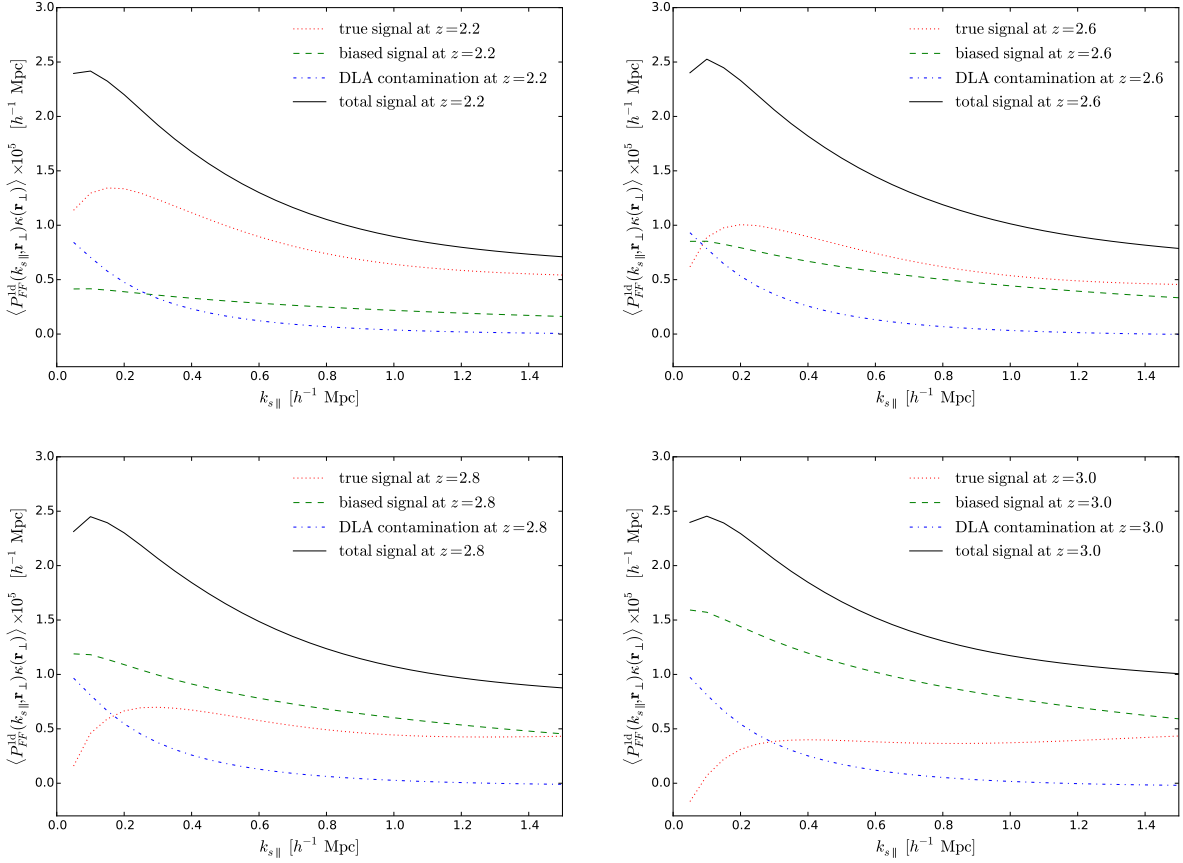


**Figure 6:** Different components of the signal of the cross-correlation between lensing convergence and the Lyman- $\alpha$  forest power spectrum at the same angular position, i.e.  $\langle P_{\text{DLA}}^{\text{1d}}(k_{s\parallel}, \mathbf{r}_{\perp}) \kappa(\mathbf{r}_{\perp}) \rangle$ . The red dotted line shows the true signal that is produced by the nonlinear gravitational evolution, the green dashed line shows the continuum-misestimation bias due to the Lyman- $\alpha$  continuum fitting, the blue dot-dashed line shows the DLA contamination, and the black solid line shows the total signal. The redshift of the signal increases from the top left to bottom right panels.

number of pixels of the  $i^{\text{th}}$  forest is a constant and noise of the forest is zero. We also include the observed Lyman- $\alpha$  forest distribution obtained from the sample in Ref. [4], hence the total weight is

$$w(k, z) = \frac{N_{\text{Lyman-}\alpha}(z)}{[P_{FF}^{\text{1d}}(k, z)]^2}, \quad (4.5)$$

where  $N_{\text{Lyman-}\alpha}(z)$  is the number of Lyman- $\alpha$  forest at  $z$ . The joint true and total signals from  $2.2 \leq z \leq 3$  are shown respectively as the blue dashed and red solid lines in figure 7, whereas the measurement in Ref. [4] is shown as the black data points with error bar. We find that the total signal is closer to the measurement than the true signal alone, but still smaller than the measurement on all scales. To better quantify the difference, we compute  $\chi^2$  using the full covariance matrix estimated in Ref. [4], and the values are shown in the legend. As there are 12 data points and without any fitting parameters, the degrees of freedom is 12.

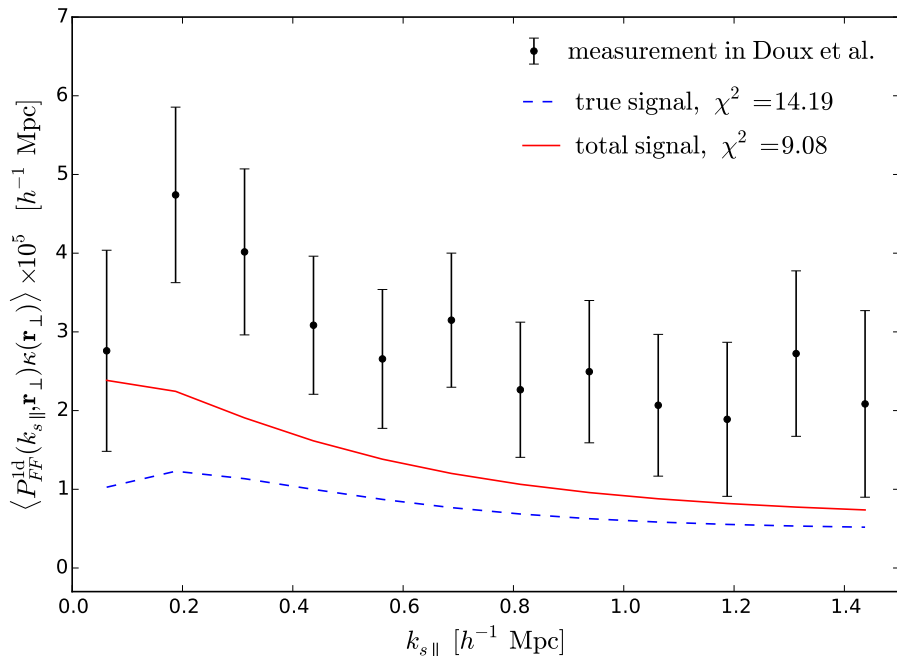


**Figure 7:** Comparison of the cross-correlation between lensing convergence and the Lyman- $\alpha$  forest power spectrum at the same angular position  $\langle P_{\text{DLA}}^{1d}(k_{s\parallel}, \mathbf{r}_\perp) \kappa(\mathbf{r}_\perp) \rangle$  between the measurement in Doux et al. (black data points with error bars) to the true (blue dashed) and total signals (red solid). The values of  $\chi^2$  computed using the full covariance matrix are shown in the legend with 12 degrees of freedom.

While the measurement is consistently larger than the total signal, we still obtain a reasonable reduced  $\chi^2$ . This is due to the high correlation between measurement points, which is shown in figure 5 of Ref. [4] and can be noticed by the lack of scatter between neighboring points. We find that the total signal gives a  $\chi^2 = 9.1$  and that neglecting the biased signal and DLA contamination worsens the fit to  $\chi^2 = 14.19$ . Therefore, even in the current data, it is important to include new effects discussed in this paper. We also note that Doux et al report best-fit  $\chi^2$  of 5.4 (which, while low, is not anomalously low with  $p = 0.9$  with 11 degrees of freedom). Their model would roughly correspond to an artificial increase in bias for our true signal, but the improvement in fit is not significant, so we cannot exclude our model as a complete model for the data. One would be able to examine this more critically with future surveys that have more and better Lyman- $\alpha$  forest measurements.

## 5 Conclusion

In this paper, we investigate the three-point function form by the cross-correlation between forest power spectrum and the CMB lensing convergence. We find that not only the gravitational evolution produces the flux-flux-lensing bispectrum, but the mis-estimation of the mean flux over the finite length of Lyman- $\alpha$  forest skewers would also generate non-zero correlation. In particular, this systematic effect dominates the underlying signal at  $z \gtrsim 2.8$ , which has to be taken into account for unbiasedly probing the gravitational effect at high redshift using this specific bispectrum.

We demonstrate that integrating the flux-flux-lensing bispectrum with full angular and scale dependences over the angular information between the forest power spectrum and the CMB lensing is equivalently to the cross-correlation between the forest power spectrum and the CMB lensing at the same angular positions, which is measured in Ref. [4]. We show that our predictions are consistent with the signal measured by Ref. [4], and the inclusion of the systematic effects from Lyman- $\alpha$  forest continuum fitting and the DLA contamination improves the agreement. However, for both with and without the systematic effects, we obtain acceptable  $\chi^2$  values. Furthermore, the reported best-fit  $\chi^2$  with one fitting parameter in Ref. [4] is low but not anomalously small.

If our prediction is correct, then one interesting implication is that while Ref. [4] shows that the effective nonlinear bias, which encodes the excess of the forest power spectrum response with respect to that of the linear field, is  $b_2^{\text{eff}} = 1.16 \pm 0.53$ , our simulations suggest it to be negative as the forest power spectrum response  $d \ln P_{FF}^{\text{ld}}(k_{s||})/d\delta$  is always smaller than the linear power spectrum response  $d \ln P_l(k)/d\delta = 68/21 - (1/3)[d \ln k^3 P_l(k)/d \ln k]$  for all redshifts and lines-of-sight (see figure 2 of Ref. [8]). This is likely due to the missing of the systematic term, hence to interpret  $b_2^{\text{eff}}$  measured in Ref. [4] as the responses of flux bias, redshift-space distortion, and the nonlinear small-scale forest power spectrum one has to account for the continuum-misestimation bias. However, given the large uncertainty from current measurement, it is challenging to draw any concrete conclusions. With future surveys such as DESI [21] that have less uncertainty, one can more critically examine this correlation as well as how the forest power spectrum responds to the overdensity gravitationally.

## Acknowledgments

We would like to thank Cyrille Doux for providing the data points and the covariance matrix of the measurement in Ref. [4]. We would also like to thank Emmanuel Schaan and the referees for useful comments on the draft. AS acknowledges insightful conversations with Andreu Font-Ribera and hospitality of the University College London where parts of this work were performed. Results in this paper were obtained using the high-performance computing system at the Institute for Advanced Computational Science at Stony Brook University. CC is supported by grant NSF PHY-1620628.

## References

- [1] F. Bernardeau, S. Colombi, E. Gaztanaga and R. Scoccimarro, *Large scale structure of the universe and cosmological perturbation theory*, *Phys. Rept.* **367** (2002) 1–248, [[astro-ph/0112551](#)].
- [2] V. Desjacques, D. Jeong and F. Schmidt, *Large-Scale Galaxy Bias*, [1611.09787](#).
- [3] M. Alvarez et al., *Testing Inflation with Large Scale Structure: Connecting Hopes with Reality*, [1412.4671](#).
- [4] C. Doux, E. Schaan, E. Aubourg, K. Ganga, K.-G. Lee, D. N. Spergel et al., *First detection of cosmic microwave background lensing and Lyman-  $\alpha$  forest bispectrum*, *Phys. Rev.* **D94** (2016) 103506, [[1607.03625](#)].
- [5] PLANCK collaboration, P. A. R. Ade et al., *Planck 2015 results. XIII. Cosmological parameters*, *Astron. Astrophys.* **594** (2016) A13, [[1502.01589](#)].

- [6] P. McDonald, *Toward a measurement of the cosmological geometry at  $Z$  2: predicting Lyman-alpha forest correlation in three dimensions, and the potential of future data sets*, *Astrophys. J.* **585** (2003) 34–51, [[astro-ph/0108064](#)].
- [7] A. Arinyo-i Prats, J. Miralda-Escudé, M. Viel and R. Cen, *The Non-Linear Power Spectrum of the Lyman Alpha Forest*, *JCAP* **1512** (2015) 017, [[1506.04519](#)].
- [8] C.-T. Chiang, A. M. Cieplak, F. Schmidt and A. Slosar, *Response approach to the squeezed-limit bispectrum: application to the correlation of quasar and Lyman- $\alpha$  forest power spectrum*, *JCAP* **1706** (2017) 022, [[1701.03375](#)].
- [9] A. M. Cieplak and A. Slosar, *Towards physics responsible for large-scale Lyman-alpha forest bias parameters*, *JCAP* **1603** (2016) 016, [[1509.07875](#)].
- [10] M. LoVerde and N. Afshordi, *Extended Limber Approximation*, *Phys. Rev.* **D78** (2008) 123506, [[0809.5112](#)].
- [11] PLANCK collaboration, P. A. R. Ade et al., *Planck 2015 results. XV. Gravitational lensing*, *Astron. Astrophys.* **594** (2016) A15, [[1502.01591](#)].
- [12] A. Slosar et al., *The Lyman-alpha forest in three dimensions: measurements of large scale flux correlations from BOSS 1st-year data*, *JCAP* **1109** (2011) 001, [[1104.5244](#)].
- [13] M. Blomqvist et al., *Broadband distortion modeling in Lyman- $\alpha$  forest BAO fitting*, *JCAP* **1511** (2015) 034, [[1504.06656](#)].
- [14] SDSS collaboration, P. McDonald et al., *The Lyman-alpha forest power spectrum from the Sloan Digital Sky Survey*, *Astrophys. J. Suppl.* **163** (2006) 80–109, [[astro-ph/0405013](#)].
- [15] C.-T. Chiang, C. Wagner, A. G. Sánchez, F. Schmidt and E. Komatsu, *Position-dependent correlation function from the SDSS-III Baryon Oscillation Spectroscopic Survey Data Release 10 CMASS Sample*, *JCAP* **1509** (2015) 028, [[1504.03322](#)].
- [16] P. McDonald, U. Seljak, R. Cen, P. Bode and J. P. Ostriker, *Physical effects on the Ly-alpha forest flux power spectrum: Damping wings, ionizing radiation fluctuations, and galactic winds*, *Mon. Not. Roy. Astron. Soc.* **360** (2005) 1471–1482, [[astro-ph/0407378](#)].
- [17] A. Font-Ribera et al., *The large-scale cross-correlation of Damped Lyman Alpha Systems with the Lyman Alpha Forest: First Measurements from BOSS*, *JCAP* **1211** (2012) 059, [[1209.4596](#)].
- [18] K. K. Rogers, S. Bird, H. V. Peiris, A. Pontzen, A. Font-Ribera and B. Leistedt, *Simulating the effect of high column density absorbers on the one-dimensional Lyman-alpha forest flux power spectrum*, [1706.08532](#).
- [19] BOSS collaboration, K. S. Dawson et al., *The Baryon Oscillation Spectroscopic Survey of SDSS-III*, *Astron. J.* **145** (2013) 10, [[1208.0022](#)].
- [20] I. Pâris et al., *The Sloan Digital Sky Survey Quasar Catalog: twelfth data release*, *Astron. Astrophys.* **597** (2017) A79, [[1608.06483](#)].
- [21] DESI collaboration, A. Aghamousa et al., *The DESI Experiment Part I: Science, Targeting, and Survey Design*, [1611.00036](#).